Influence of Prandtl number on stability of mixed convective flow in a vertical channel filled with a porous medium

P. Bera, and A. Khalili

View Online   Export Citation

ARTICLES YOU MAY BE INTERESTED IN

Stability of mixed convection in an anisotropic vertical porous channel
Physics of Fluids **14**, 1617 (2002); https://doi.org/10.1063/1.1460879

Weakly nonlinear stability analysis of non-isothermal Poiseuille flow in a vertical channel
Physics of Fluids **27**, 064103 (2015); https://doi.org/10.1063/1.4922342

Bifurcation and instability of annular Poiseuille flow in the presence of stable thermal stratification: Dependence on curvature parameter
Physics of Fluids **31**, 104105 (2019); https://doi.org/10.1063/1.5122289
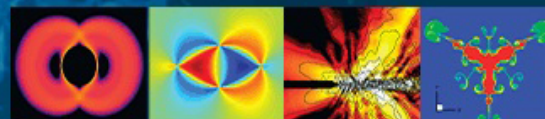
AIP Publishing

Influence of Prandtl number on stability of mixed convective flow in a vertical channel filled with a porous medium

P. Bera
Indian Institute of Technology Roorkee, Roorkee 247 667, India

A. Khalili[a)]
Max Planck Institute for Marine Microbiology, 28359 Bremen, Germany
and International University Bremen, 28759 Bremen, Germany

Buoyancy opposed mixed convection is considered in a vertical channel filled with an isotropic, porous medium, in which the motion of an incompressible fluid is induced by external pressure gradients and buoyancy forces. The Brinkman-Wooding-extended Darcy model has been used to study the instability mechanisms of the basic flow and its dependence on the Prandtl number (Pr) of the fluid. The stability analysis indicated that for the same Reynolds number (Re), the fully developed base flow was highly unstable for a fluid with high Pr. For a porous medium with a Darcy number (Da) of 10^{-6} and $\mathrm{Pr} \geq 0.7$, two different types of instability, Rayleigh-Taylor (R-T) and buoyant instability, are observed. The R-T instability mode is observed for relatively small values of Re. Further, the results show that for $\mathrm{Da}=10^{-5}$ and $\mathrm{Pr}<1$, the spectrum of the energy profile is abrupt and sudden, whereas the same is smooth when $\mathrm{Da}=10^{-6}$. In the case of R-T instability, the critical value of Ra at low Re is given by $-2.47/\mathrm{Da}$. Though the R-T mode of instability is independent of Pr, the range of Re that sustains the R-T mode is a function of Pr. It has been found that enhancement of Pr reduces the Re range mentioned above. In contrast to the case of a purely viscous fluid, where the effect of Pr is not significant, in isotropic porous media Pr plays a significant role in characterizing the flow stability. The instability characteristics of zero temperature flux perturbation (BC-I) and zero heat flux perturbation (BC-II) on the boundaries differ significantly in the case of the R-T stability mode. However, both conditions lead to similar results for buoyant stability, except at small values of Re. © *2006 American Institute of Physics*.
[DOI: 10.1063/1.2405321]

I. INTRODUCTION

Thermal convection in porous media is a topic of fundamental interest in diverse fields, such as thermal insulation engineering, transpiration cooling, geothermal reservoir dynamics, and marine biological science (hydrothermal vents in shallow water seas, convection in melting snow, flow in biological membranes and filters).

The majority of the available studies are relevant to free convective heat transfer. However, it is known that the fluid trapped in pores is subject to vaporization, condensation or migration, giving rise to mixed convection phenomena. For example, convection in permeable sediment of hot vents is a combination of forced and natural convection. Due to high pressure gradients, the hot water masses move upward leading to a forced convection mechanism. In the presence of a gravitational field, however, the temperature gradient, along with the density gradients in the fluid induce varying body forces, which in turn, cause natural convection.[1–3] This problem constitutes a very new research area, and its theoretical investigation has been largely overlooked. Several attempts have been made by different scientists in the area of natural or forced convection, and are well documented in a book by Nield and Bejan.[4]

In the case of laminar flows, few investigations in wall bounded mixed convection through a vertical channel filled with a porous medium are reported elsewhere.[5–8] If flow instability and transition occur, however, the fluid flow and heat transfer mechanisms may significantly differ from those obtained for laminar flows. An example for this is a recent study of Bera and Khalili[9] on the stability of mixed convection in a vertical channel filled with an anisotropic porous medium. They suggested that fully developed 1D buoyancy assisted flow within a constant pressure gradient does not remain 1D beyond a critical heat source intensity. It was also found that (i) the least stable mode is two-dimensional, (ii) fully developed base flow is highly unstable (stable) for high (low) permeable porous media as well as for media with small (large) thermal conductivity, and (iii) for small Darcy numbers the effect of the Forchheimer term is negligible. Similar findings were also reported by Chen[10] while studying the stability of buoyancy assisted mixed convection in the same geometry filled with an isotropic porous medium.

The present paper is concerned with buoyancy-*opposed* mixed convection in a similar geometry. The instability mechanism for different fluids was studied in an isotropic porous medium. A wide range of Prandtl numbers [0.01,

---
[a)]Author to whom correspondence should be addressed. Electronic mail: akhalili@mpi-bremen.de
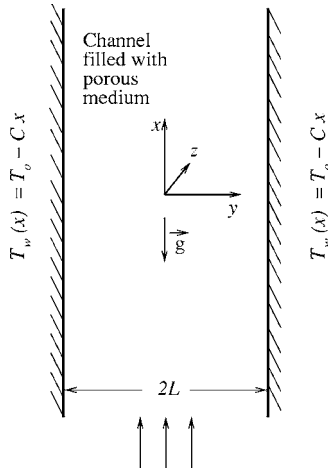
FIG. 1. Schematic of the problem considered.

100] were considered to simulate the stability characteristics of fluids covering the range of light liquids to heavy oils. As the Darcy model does not hold for high velocities and permeabilities, the Brinkman-Forchheimer-Wooding-extended Darcy model[11–19] was employed.

At the channel walls, two different types of boundary conditions for perturbed temperature are possible. If the bounding walls of the fluid layer have a high heat conductivity and a large heat capacity, then temperature would be spatially uniform and constant in time. In other words, the temperature of the boundary would be stable despite any flow or temperature perturbation in the fluid domain. Therefore, taking the disturbed wall temperature equal to zero (boundary condition of first kind) would be appropriate. In what follows, this case is termed as BC-I. However, this fixed temperature boundary condition at the surface of the fluid layer may be too restrictive, because there will be heat exchange between the solid conductive wall and the fluid. Hence, a constant heat flux at the wall could also be possible (BC-II). This paper is organized as follows: In Sec. II, the mathematical formulation of the physical problem including base flow, disturbance, energy spectrum analysis, and code validation are described. Results and discussion including impact of Prandtl number as a function of Re and Da for BC-I and BC-II are then reported in Sec. III. Finally, some important features of the analysis are summarized in Sec. IV.

II. PHYSICAL PROBLEM AND MATHEMATICAL FORMULATION

The flow investigated here is a mixed convection problem caused by the combined action of buoyancy-opposed forces and external pressure gradients in a vertical channel of width $2L$ (see Fig. 1). The channel was bounded by two walls and filled with an isotropic porous medium. The wall temperature (T_w) was linearly varying with x as $T_w = T_o - Cx$, where C is a positive constant and T_o is the upstream reference wall temperature. The gravitational force is aligned in the negative x direction. The thermophysical properties of the fluid are assumed constant except for density dependency

of the buoyancy term in the momentum equation. The permeability, as well as thermal diffusivity of the medium, are denoted by K and k, respectively.

Using nondimensional quantities $y^* = y/L$, $x^* = x/L$, $z^* = z/L$, $\mathbf{V}^*(v, u, w) = \mathbf{V}/\bar{U}_0$, $P^* = P/\rho\bar{U}_0^2$, $t^* = t\bar{U}_0/L$, $\Theta = (T - T_w)/CL \, \mathrm{Pr} \, \mathrm{Re}$, $\mathrm{Da} = K/L^2$, $\Lambda = \tilde{\mu}/\mu$, $\mathrm{F} = C_F L/K^{1/2}$, $\sigma = (\rho c)_m/(\rho c_P)_f$, $\mathrm{Pr} = \nu/k$, $\mathrm{Re} = \bar{U}_0 L/\nu$, and $\mathrm{Ra} = g\beta_T C L^4/\nu k$, the nondimensional governing equations are given by

$$\nabla \cdot \mathbf{V} = 0, \tag{1}$$

$$\frac{1}{\varepsilon}\frac{\partial \mathbf{V}}{\partial t} + \frac{1}{\varepsilon^2}(\mathbf{V} \cdot \nabla)\mathbf{V}$$

$$= -\nabla P - \frac{1}{\mathrm{Da}\,\mathrm{Re}}\mathbf{V} - \mathrm{F}|\mathbf{V}|\mathbf{V} + \frac{\mathrm{Ra}}{\mathrm{Re}}\Theta\mathbf{e_x} + \frac{\Lambda}{\mathrm{Re}}\nabla^2\mathbf{V}, \tag{2}$$

$$\sigma\frac{\partial \Theta}{\partial t} + u\frac{\partial \Theta}{\partial x} + v\frac{\partial \Theta}{\partial y} + w\frac{\partial \Theta}{\partial z}$$

$$= \frac{1}{\mathrm{Re}\,\mathrm{Pr}}\left(\frac{\partial^2 \Theta}{\partial x^2} + \frac{\partial^2 \Theta}{\partial y^2} + \frac{\partial^2 \Theta}{\partial z^2} - u\right) \tag{3}$$

in which $\mathbf{V} = (u, v, w)$, Θ, and P are the nondimensional velocity vector, temperature, and pressure, respectively. Furthermore, $\bar{U}_0$ is the mean base velocity, $\mathbf{e_x}$ is the unit vector along x, β_T is volumetric thermal expansion coefficient, Λ is the viscosity ratio, ϵ is porosity, and σ is the heat capacity ratio. Different values have been reported for μ_e in the literature.[19,20] However, in the absence of any specifically measured values, a value of $\Lambda = 1$ has been assigned for this study.

The nondimensional governing parameters are Rayleigh number (Ra), Reynolds number (Re), Prandtl number (Pr), Forchheimer number (F), and Darcy number (Da).

A. Base Flow

The base flow is a fully developed, unidirectional, steady, and laminar flow. Under these circumstances the governing equations (1)–(3) are reduced to

$$-\mathrm{F}\,\mathrm{Re}|U_0|U_0 - \mathrm{Re}\frac{dp}{dx} - \frac{1}{\mathrm{Da}}U_0 + \mathrm{Ra}\,\Theta_0 + \Lambda\frac{d^2U_0}{dy^2} = 0, \tag{4}$$

$$U_0 = \frac{d^2\Theta_0}{dy^2}, \tag{5}$$

accompanied with the boundary conditions

$$U_0 = \Theta_0 = 0 \quad \text{at } y = \pm 1, \tag{6}$$

with U_0 and Θ_0 being the basic velocity and temperature, respectively. The nonlinear coupled equations (4) and (5) are solved numerically using the DBVPFD routine of the IMSL library. In the case of F=0, the same is solved analytically. The analytical solution of the above equations is given by

$$\Theta_0 = \frac{e_2}{b_1}\left(\left(1 - \frac{1}{d}\right)\frac{\cosh m_2 y}{\cosh m_2} + \frac{1}{d}\frac{\cos m_3 y}{\cos m_3} - 1\right), \tag{7}$$

$$U_0 = \frac{e_2}{b_1}\left(\left(1-\frac{1}{d}\right)m_2^2\frac{\cosh m_2 y}{\cosh m_2} - \frac{m_3^2}{d}\frac{\cos m_3 y}{\cos m_3}\right). \quad (8)$$

The parameters denoted by b_1, d, e_2, m_2, and m_3 are given by $-\mathrm{Ra}/\Lambda$, $1+m_3^2/m_2^2$, $(b_1 d m_2)/[m_3(m_3 \tanh m_2 - m_2 \tan m_3)]$, $[(a+\sqrt{a^2+4b_1})/2]^{1/2}$, and $[(-a+\sqrt{a^2+4b_1})/2]^{1/2}$, respectively, in which a is defined by $1/(\Lambda\,\mathrm{Da})$.

B. Disturbance and energy spectrum

Here, the linear stability of a fully developed unidirectional base flow is studied using standard techniques.[21]

Using infinitesimal disturbances to the fully developed laminar base flow, the solution of the 3D problem can be written as

$$(\mathbf{V}, P, \Theta) = (U_0(y)\mathbf{e_x}, P_o(x), \Theta_o(y)) + (\mathbf{V}', P', \Theta'). \quad (9)$$

The primed quantities denote the infinitesimal disturbances on the corresponding terms and can be represented by $(\mathbf{V}', P', \Theta')^T = e^{i(\alpha x+\beta z-\alpha c t)}(\hat{\mathbf{V}}, \hat{P(y)}, \hat{\Theta(y)})^T$, with α and β as the real-valued wave numbers in the x and z direction, respectively, and $c=\hat{c}_r+i\hat{c}_i$ is the complex wave speed. The growth and decay of the disturbances depend on $\hat{c}_i$. The details of this method can be found elsewhere.[9]

To understand the physical mechanisms responsible for the instability, the two-dimensional ($\beta=0$) disturbance kinetic and thermal potential energy balances were studied first. The rate of change of nondimensional kinetic and thermal energies are

$$\frac{1}{\varepsilon}\frac{\partial}{\partial t}\left\langle\frac{1}{2}(u'^2+v'^2+w'^2)\right\rangle$$
$$=\frac{1}{\varepsilon^2}\left\langle-u'v'\frac{dU_0}{dy}\right\rangle+\frac{\mathrm{Ra}}{\mathrm{Re}}\langle u'\Theta'\rangle$$
$$-\frac{1}{\mathrm{Da\,Re}}\langle(u'^2+v'^2+w'^2)\rangle$$
$$-\mathrm{F}\langle|U_0|(2u'^2+v'^2+w'^2)\rangle-\frac{\Lambda}{\mathrm{Re}}[\langle(\nabla u')^2$$
$$+(\nabla v')^2+(\nabla w')^2\rangle]=E_s+E_b+E_D+E_F+E_d, \quad (10)$$

$$\sigma\frac{\partial}{\partial t}\left\langle\frac{1}{2}\Theta'^2\right\rangle=\frac{1}{\mathrm{Re\,Pr}}\left\langle-\left[\left(\frac{\partial\Theta'}{\partial x}\right)^2+\left(\frac{\partial\Theta'}{\partial y}\right)^2\right.\right.$$
$$\left.\left.+\left(\frac{\partial\Theta'}{\partial z}\right)^2\right]\right\rangle+\left\langle-\left(\Theta'v'\frac{d\Theta_0}{dy}\right)\right\rangle$$
$$-\frac{1}{\mathrm{Re\,Pr}}\langle\Theta'u'\rangle=T_d+T_c+T_b. \quad (11)$$

Here, the brackets $\langle\rangle$ represent the volumetric average over the volume of the disturbance wave. The first term on the right-hand side of Eq. (10) is E_s, and represents the gain (loss) of the disturbance kinetic energy from (to) the mean flow through Reynolds stress, referred to as shear production (destruction). The second term denoted by E_b represents the nonisothermal effects, that is the production (destruction) of

disturbance kinetic energy caused by the action of buoyancy. The third, fourth, and fifth terms (namely E_D, E_F, and E_d) are negative definite quantities representing the dissipation of disturbance kinetic energy due to surface drag, form drag, and viscous effects, respectively.

The terms T_d and T_c in Eq. (11) are negative and positive definite quantities, respectively. They represent the dissipation of disturbance thermal energy due to diffusion and the production of disturbance thermal energy due to thermal convection. Finally, the last term, denoted by T_b represents the production (dissipation) of disturbance thermal energy due to buoyancy.

The relative error in the kinetic energy balance, δ_K, is defined as the residual, normalized by the sum of the absolute values of shear production of disturbance kinetic energy and disturbance kinetic energy due to thermal buoyant potential, and is given by

$$\delta_K=\frac{|E_s+E_b+E_D+E_F+E_d|}{|E_s|+|E_b|},$$

while

$$\delta_T=\frac{|T_c+T_d+T_b|}{\max\{|T_c|,|T_d|,|T_b|\}}$$

is used to account for the relative error of the thermal energy balance.

C. Validation of code

Verification of the code was shown in several ways. First, the independence of the solution was examined for variation of grid size (M) and order of the base polynomial (N). Second, it was checked whether or not the total rate of change of kinetic and thermal energy at critical points were zero. Finally, some comparisons of our data with published results were made for specific choices of input parameters.

As can be seen from Table I, grid independence of the numerical simulation was achieved at $M=701$. Table II shows the convergence of the Galerkin method at Re $=15\,000$ and F=0. With an order of polynomial (N) of 25 and 30, an accuracy up to five digits after the decimal point can already be obtained. As the number of terms in the approximations increased, the results remained consistent and accuracy also improved. Similarly, satisfactory results were obtained for other sets of input parameters. In all computations reported, it was found that accurate solutions could be reached by taking 50 terms of the Lagrangian polynomials. An additional check was provided via analysis of the energy balance. As demonstrated in Table III for all calculations presented in this paper, the errors in thermal energy balance (δ_T) and kinetic energy balance (δ_K) were $\leq 2\%$. Due to these low errors, one may conclude that the flow and stability features are well resolved. Finally, in the linear stability analysis given below, 701 grid points and an order of polynomial of 50 have been considered as standard values for all calculations.

The final check was made by a comparison between the published results for a fluid-filled vertical channel as a particular case of our general purpose study. Table IV compares

TABLE I. Dependence of the critical Rayleigh number on number of grid points (M) at $N=50$ ($\Lambda=1$, $\epsilon=0.4$, F=0, Pr=7, and Da=10^{-6}).

Re	Grid No.	Ra	α
10^4	201	−1815000	7.14
10^4	301	−1805000	7.20
10^4	401	−1805000	7.24
10^4	501	−1805000	7.30
10^4	601	−1805000	7.25
10^4	701	−1805000	7.26
10^4	801	−1805000	7.26
5×10^4	201	−367000	3.40
5×10^4	301	−365000	3.36
5×10^4	401	−365000	3.42
5×10^4	501	−367000	3.34
5×10^4	601	−367500	3.26
5×10^4	701	−367500	3.26
5×10^4	801	−367500	3.26
10^5	201	−209500	1.98
10^5	301	−209500	2.00
10^5	401	−212500	1.98
10^5	501	−213000	1.98
10^5	601	−213000	1.98
10^5	701	−213000	1.98
10^5	801	−213000	1.98

TABLE III. Kinetic and thermal energy errors for different values of the Prandtl number (Re=50 000, Da=10^{-6}, F=0, $\Lambda=1$, and $\epsilon=0.4$).

Pr	Re	$\delta_K(\%)$	$\delta_T(\%)$	Ra	α
0.7	5×10^3	0.2	0.030	−6167500	30.06
0.7	5×10^4	0.001	0.164	−2250625	2.7
0.7	10^5	0.0004	0.315	−1486250	1.98
7	5×10^3	0.0005	0.546	−3181250	11.98
7	5×10^4	0.0004	0.862	−367500	3.26
7	10^5	0.0002	1.401	−213000	1.98
70	5×10^3	0.0001	0.641	−702500	12.68
70	5×10^4	0.0003	1.202	−39500	3.22
70	10^5	0.001	1.800	−22250	1.94

the critical Ra and α of the present study with those by Chen and Chung[22] for $\varepsilon=1$, Da=10^6, and Pr=0.7. As can be seen, the agreement is good.

III. RESULTS AND DISCUSSIONS

In the study presented here, linear theory of stability analysis has been used to study the conditions necessary for the occurrence of the maximum stability of different fluids in a vertical channel filled with porous medium. All calculations made here use a porosity $\epsilon=0.4$, a viscosity ratio $\Lambda=1$, and a heat capacity ratio $\sigma=1$. The effect of Prandtl number (Pr) on the stability of base flow was emphasized by taking three different values of Pr (0.7, 7.0, and 70). With this, the stability characteristics of air, water and oil could be studied in a low permeable porous medium (Da=10^{-6}). Fur-

thermore, Reynolds number (Re) has been employed to find the neutral stable mode. Throughout this section, critical Ra_c and α_c values have been represented by Ra and α, respectively, and a logarithmic scale has been used along the vertical axis to display all the instability boundaries on the (Re, |Ra|) plane. From rigorous numerical experimentation, it has been concluded that, similar to buoyancy assisted flow,[9] two-dimensional disturbance motion causes the maximum instability of buoyancy opposed mixed convective flow in the vertical channel (data not shown here). Therefore in the entire present section, except for the critical Ra of Rayleigh-Taylor instability mode,[21] $\beta=0$ has been considered.

As mentioned by Chen and Chung,[22] two different conditions are possible at the boundaries: (i) zero temperature perturbation (BC-I), and (ii) zero heat flux perturbation (BC-II). In the following, the impact of Prandtl number on the stability of base flow under BC-I (corresponding to systems with highly conducting walls) followed by the same under BC-II is investigated. A comparison of results under two different temperature perturbation conditions is also made.

To find out the role of the Forchheimer term on the instability boundaries, a Darcy-Brinkman-Wooding-Forchheimer model (DBWF) with different values for the Forchheimer number (F) as well as a Darcy-Brinkman-Wooding (DBW) model were employed. The plot of the instability boundary curves as a function of Re at Da=10^{-6} (see Fig. 2) showed that the influence of the Forchheimer number is a simple vertical shift rather than a modification of the profiles. Therefore, F=0 has been assigned for the entire section.

TABLE II. Dependence of complex growth speed on the order of the base polynomials (N) for Da=10^{-6}, Pr=1, F=0, $\Lambda=1$, and $\epsilon=0.4$.

N (order of polynomial)	c_r	c_i
10	1.18888252	−0.00074394
20	1.18897272	−0.00081439
25	1.18896191	−0.00084331
30	1.18895945	−0.00083926
35	1.18896062	−0.00083974
40	1.18896068	−0.00083964
45	1.18896056	−0.00083956
50	1.18896058	−0.00083952
55	1.18896061	−0.00083952
60	1.18896069	−0.00083951

TABLE IV. Comparison between published results (Ref. 22) and present results ($\epsilon=1$, Pr=0.7, Da=10^{-7}).

Re	Ra Present work	Ra Cheng[a]	α Present work	α Cheng[a]
660	−6.03	−6.06	1.27	1.275
1000	−4.58	−4.58	1.20	1.20
1750	−2.77	−2.74	1.10	1.11
2500	−1.62	−1.54	1.06	1.065

[a]Reference 22.
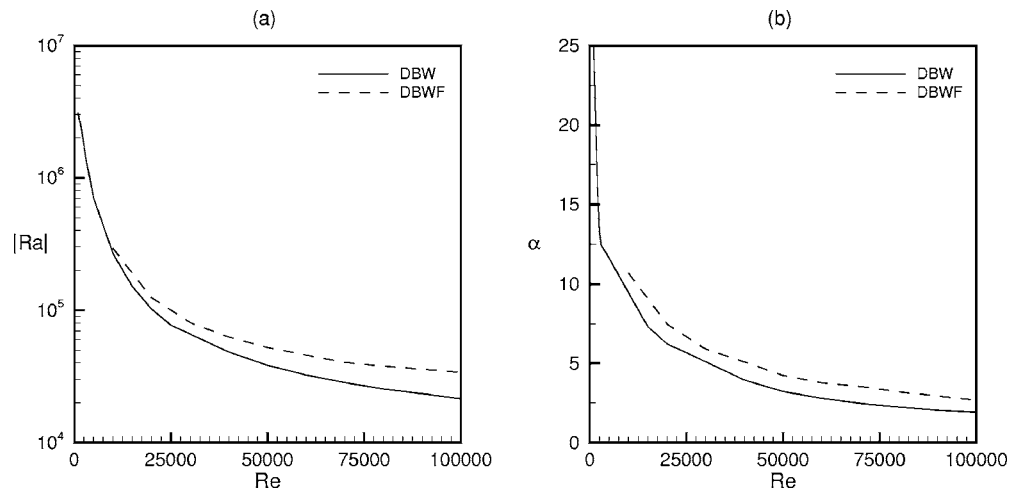
FIG. 2. Dependence of the critical Rayleigh number (a) and wave number (b) on Re for different models for Da=10^{-6} and Pr=70.

Furthermore, a special note must be made regarding the Reynolds number. As mentioned by many researchers,[11–17] for a porous environment, different characteristic lengths may be chosen as an input for the Reynolds number. Usually, Re is based on macroscopic lengths such as depth, width or height of the geometrical configuration in question. However, as mentioned by Ward,[23] it has been customary to introduce a "superficial" Reynolds number based on the permeability of the medium. Some authors have also introduced a pore-scale Reynolds number based on the average grain or pore diameter.[4] Obviously, the inclusion of one or the other length scale will lead to a different magnitude of the corresponding Re. Hence in our case, a Re of 50 000, based on the half channel width (L), is equivalent to Re=50, based on the square root of permeability (when Da=10^{-6} and L=5 cm). However, to remain consistent with past studies, a channel width-based definition of Re was chosen in this study.

A. Zero temperature perturbation

Figures 3(a) and 3(b) illustrate the instability boundaries on (Re, |Ra|) and (Re, α) planes for different fluids in an isotropic porous medium. As can be observed from Fig. 3(a), a higher Pr results in a lower critical Ra. That is, the effect of Pr is destabilizing.

A qualitative explanation for the physics involved is provided by examination of the diffusion terms in the momentum and energy equations. The importance of momentum and thermal diffusion are measured by $(Re)^{-1}$ and $(Re\,Pr)^{-1}$. Thus, Prandtl number reveals the relative efficiency of momentum and thermal diffusion. Hence, a low Pr includes an increase in the thermal diffusivity, which itself suppresses the thermal fluctuations in the flow field. As a result, the flow remains stable even for larger values of Ra. However, the situation reverses when a fluid with a high Prandtl number is considered. Since an increase in Pr increases the interaction between the substance and the fluid particles, the flow strength in the channel is reduced.[24]

To understand the possible underlying mechanism, a study of the energy spectrum of different fluids as a function of Reynolds number is required. It has been observed that for Pr=0.7 and 70, the production disturbance kinetic energy due to buoyancy force (E_b) is the dominating term in balanc-
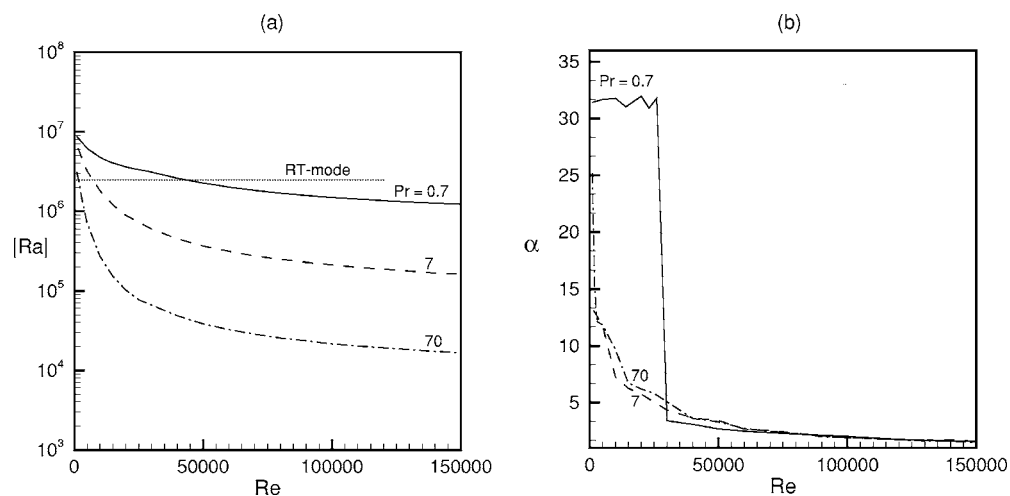
FIG. 3. Dependence of the critical Rayleigh number (a) and wave number (b) on Re for different Prandtl numbers and Da=10^{-6}.

(a) Pr = 0.7

(a) Pr = 70

Tempe rature

$\Theta_{max} = 0.39$

$= 1.4$
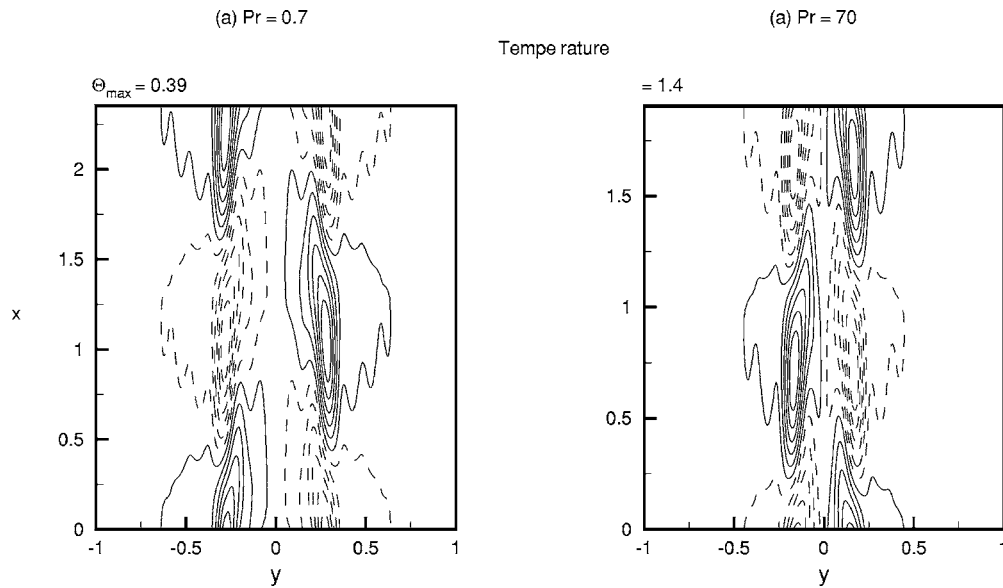
FIG. 4. The disturbance temperature for Re=50 000, Da=10^{-6}; (a) Pr=0.7 (Θ_{min}=−0.39, Θ_{max}=0.39) and (b) Pr=70 (Θ_{min}=−1.4, Θ_{max}=1.4) within one period.

ing the dissipation of kinetic energy due to surface drag (E_D) throughout the Re range. Whereas, the thermal energy spectrum for the same set of Pr shows that the diffusion of thermal energy (T_d) is balanced by the production of disturbance thermal energy due to convection (T_c) in almost the entire Re range (data are not shown). However it remains unclear why the critical value of Ra and α change significantly. The clue to this was given when both stream functions and temperature profiles were calculated (see Figs. 4 and 5). It is not the qualitative shift of the isotherms towards the center which is responsible for the phenomenon mentioned above, but rather the quantitative, sudden jump of the values of Θ_{max} varying from 0.39 (for Pr=0.7) to 1.4 (for Pr=70) shown in Figs. 4(a) and 4(b). Although a similar jump is experienced by

Ψ_{max} (see Fig. 5), the flow stability is decided by the strength of the thermal convection. Therefore, enhancement of Pr increases the strength of the disturbance temperature, which in turn, makes the system unstable even at a low Ra.

An important feature of the instability boundaries on the (Re, |Ra|) plane is that, for all cases, but especially for water (Pr=7) and heavy oil (Pr=70), a drastic change of Ra is observed before a threshold value of Re is reached [Fig. 3(a)]. Beyond this value, a smooth and slow change occurs. This is because the fluid is unstably stratified in the vertical direction when there is no motion. At low Re with a minimum heat source intensity, however, an instability occurs because hot fluid from the bottom and cold fluid from top (due to back flow) accelerate towards each other. This type

(a) Pr = 0.7

(a) Pr = 70

Stream lines

$\Psi_{max} = 0.061$

$= 0.004$
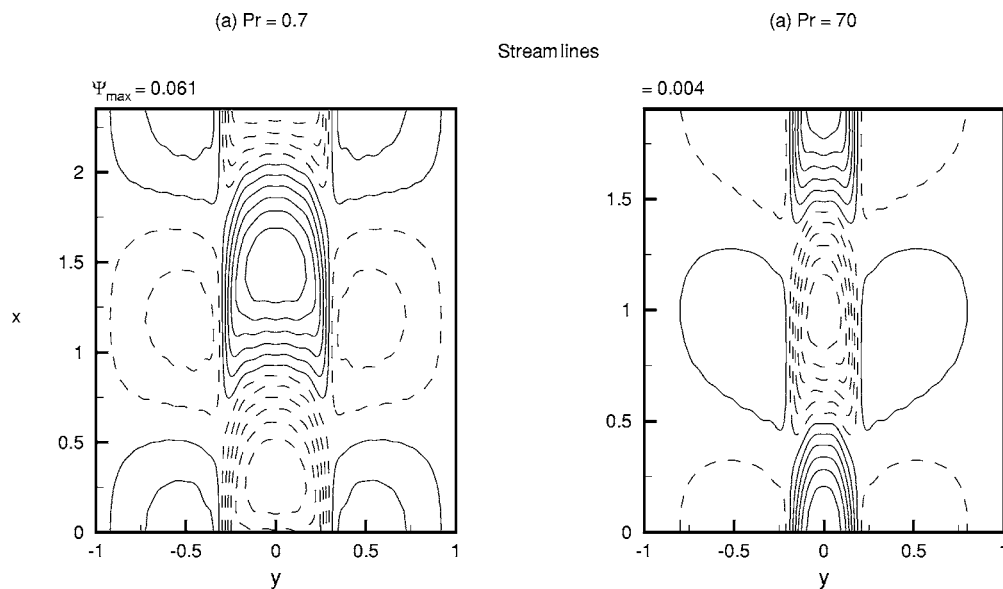
FIG. 5. The disturbance streamlines for Re=50 000 and Da=10^{-6}; (a) Pr=0.7 (ψ_{min}=−0.06, ψ_{max}=0.06) and (b) Pr=70 (ψ_{min}=−0.005, ψ_{max}=0.005) within one period.

TABLE V. Dependence of the critical Rayleigh number of the Rayleigh-Taylor instability mode on the Darcy number.

Da	$-$Ra
10^{-2}	246.5767637
10^{-3}	2465.4766637
10^{-4}	24654.6282764
10^{-5}	246553.15399170
10^{-6}	2465476.60827637
10^{-7}	24650791.16821289

of instability is known as the Rayleigh-Taylor instability, through which a slow flow can carry denser fluid upwards into the region of lighter fluid. Such an instability was also observed by Yao and Rogers.[25]

Besides energy due to shear force existing in the viscous fluid, for a channel filled with a saturated porous medium, a new source of disturbance energy (namely the one caused by surface drag) appears in the region of low velocity. The consequence of this is a back flow close to the bounding walls leading to the appearance of separation points in the near-wall region. From this state, even a minor enhancement of

Re is sufficient to increase the convection in the main flow direction. With this, a more dense fluid can then be transported upwards to destabilize the flow, and the critical Ra falls significantly.

The critical value of Ra has been calculated as a function of Da, and is shown in Table V. It can be seen therein that the RT mode of instability is achieved when Ra Da$=-2.47$. To shed more light on the mechanism leading to the Rayleigh-Taylor flow instability, rigorous numerical experiments were carried out on the basic flow profile as a function of three governing parameters Ra, Da, and Λ. Basic velocity profiles are plotted for Da$=10^{-3}$ and 10^{-6} for three different values of Ra Da, namely, -2.25, -2.5, and -2.75 [see Figs. 6(a)–6(c)]. For Ra Da$=-2.25$, no point of separation occurred. However, separation points appeared for $-$Ra Da≥ 2.5. To visualize this in more detail, the graphs were magnified at the boundary and are plotted in Figs. 6(d)–6(f). From rigorous numerical experiments on the base flow, it can be concluded that when Ra Da≈ -2.5, irrespective of any Da lying within $[10^{-2}, 10^{-7}]$, points of separation developed near the boundary walls. This suggests that in the Rayleigh-Taylor instability mode, there exists a direct link between the critical Ra and the product $-$Ra Da. Hence, reconsidering Fig. 3(b), the jumps of critical wave number for
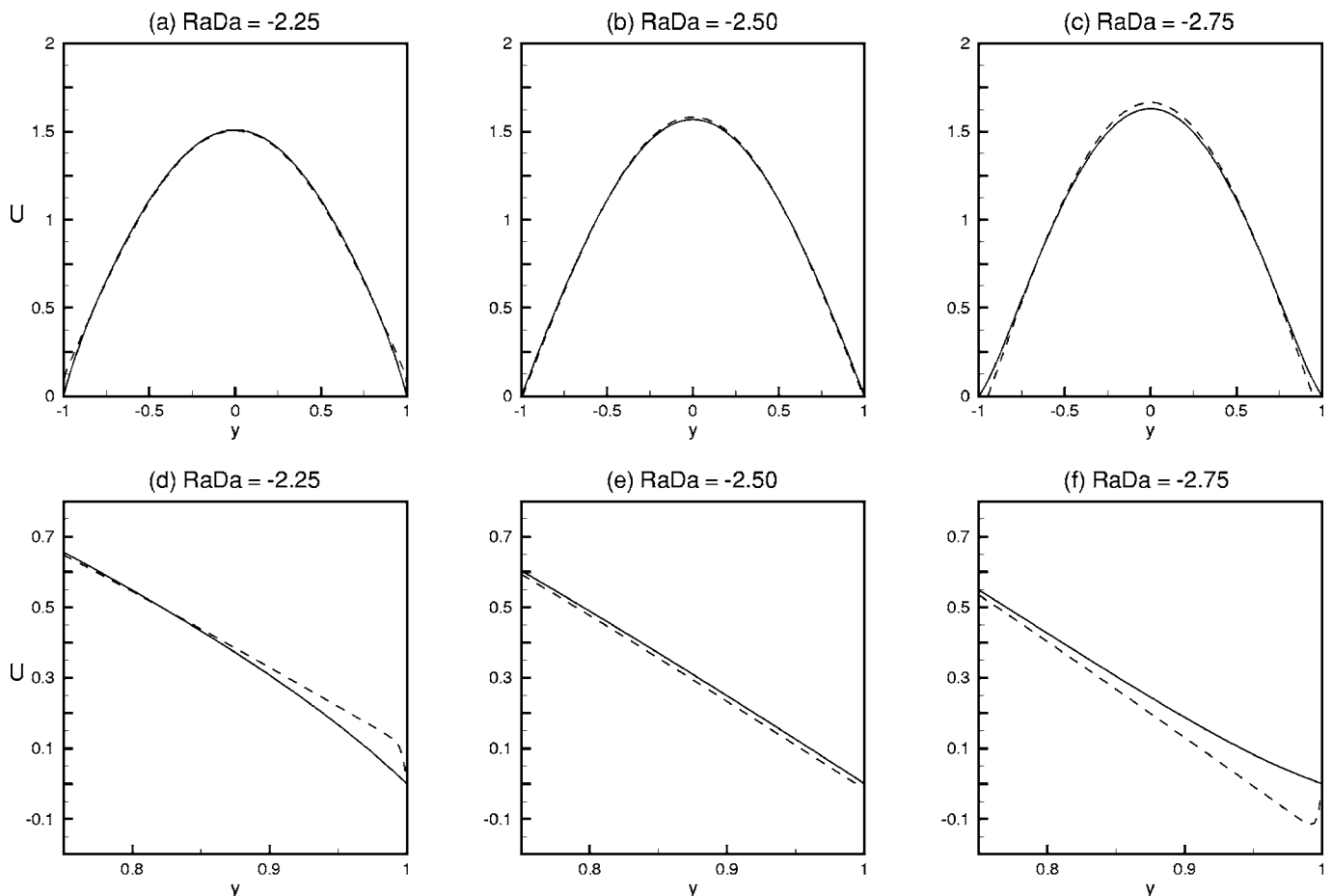
FIG. 6. Velocity profiles of basic flow (solid lines: Da$=10^{-3}$ and dotted lines: Da$=10^{-6}$). (a) Da Ra$=-2.25$, (b) Da Ra$=-2.50$, (c) Da Ra$=-2.75$. The subfigures (d), (e), and (f) are, respectively, closeups of (a), (b), and (c) near the boundary.
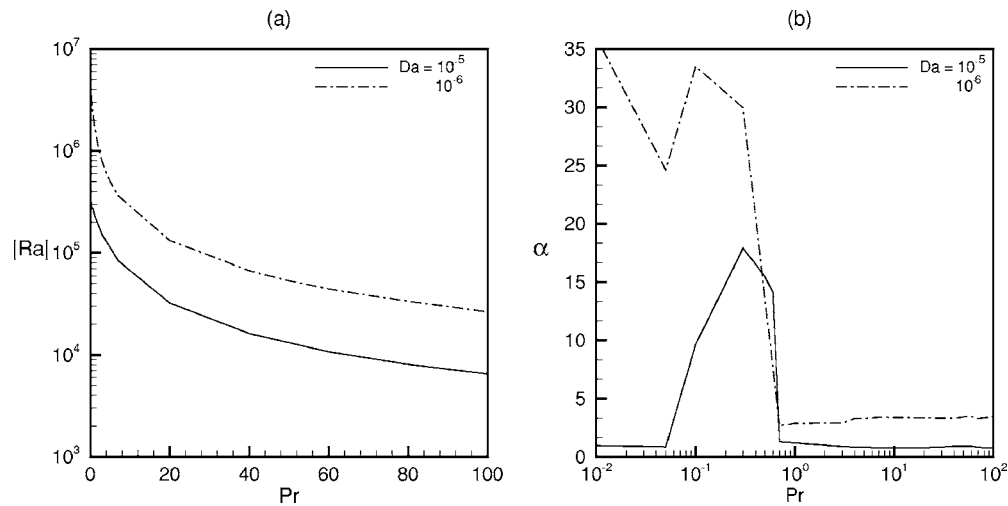
FIG. 7. Dependence of the critical Rayleigh number (a) and wave number (b) on Pr for two different values of Darcy numbers at Re=50 000.

Pr=0.7 at Re=30 000, Pr=7, at Re=10 000, and Pr=70, at Re=2000 become plausible. Similar findings were observed for fluid-filled channels[22] and tubes.[26]

Investigation of the effect of Prandtl number on flow stability for two different permeabilities (10^{-6} and 10^{-5}) at Re=50 000 (Fig. 7) disclosed two facts. First, enhancement of Pr destabilized the base flow rapidly up to a certain threshold value of Pr. Further, the critical value of Ra was reduced smoothly and slowly. Second, an increase in permeability reduced the flow stability drastically. Since an increase in permeability implies more flow into the system (equivalent to strengthening the convective flow), a slight increase of Re enhances the convection in the main flow direction. Consequently, more fluid can be transported upwards to destabilize the flow, which is shown by a fall of the critical heating condition.

The former observation can be explained with the help of an energy spectrum (Fig. 8), which shows negligible kinetic energy due to shear and viscous forces, and simultaneously a significant production of kinetic energy by buoyant force for Pr>1. However, as Pr was moved below unity, contributions arise from energy production due to shear force and energy dissipation due to a viscous term.

An interesting finding from this analysis is that shear production (E_s for Pr $\geq$ 0.7) favors of flow stabilization, whereas flow is destabilized below this. Accordingly, for Da=10^{-5}, the mode of instability changes abruptly from buoyant to shear and later to buoyant instability. In the case of Da=10^{-6} however, instability changes smoothly from shear to buoyant instability. It is interesting to note that the abrupt change in instability mode for Da=10^{-5} is related to a position in the (α-Pr) plane where α experienced a jump [Fig. 7(b)].

B. Zero heat flux perturbation

In this section, we present a brief study of instability boundaries on the (Re, $|$Ra$|$) plane and their dependency on Pr. Here, the derivatives of the temperature perturbation with respect to y at the boundaries were zero, but the temperature
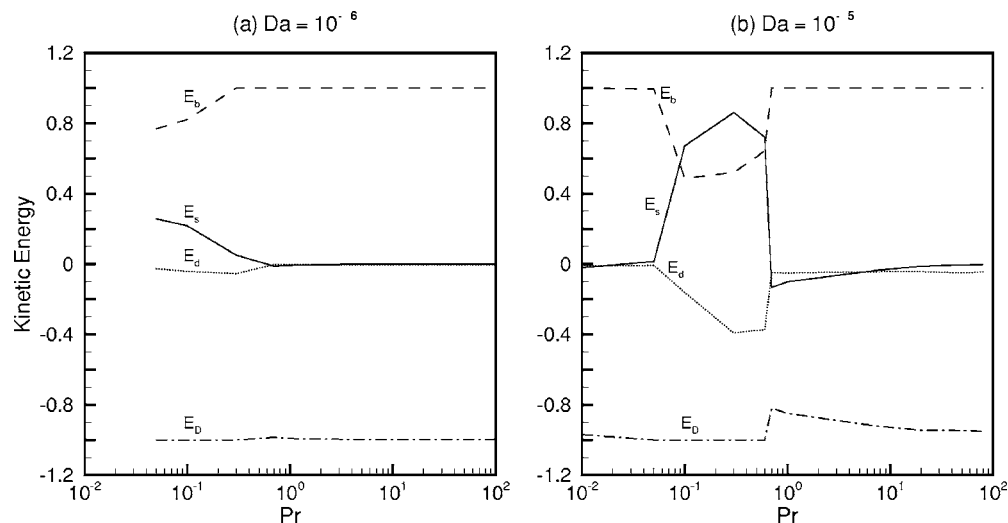
FIG. 8. Kinetic energy spectrum as a function of Pr for Re=50 000; (a) Da=10^{-6}, (b) Da=10^{-5}.
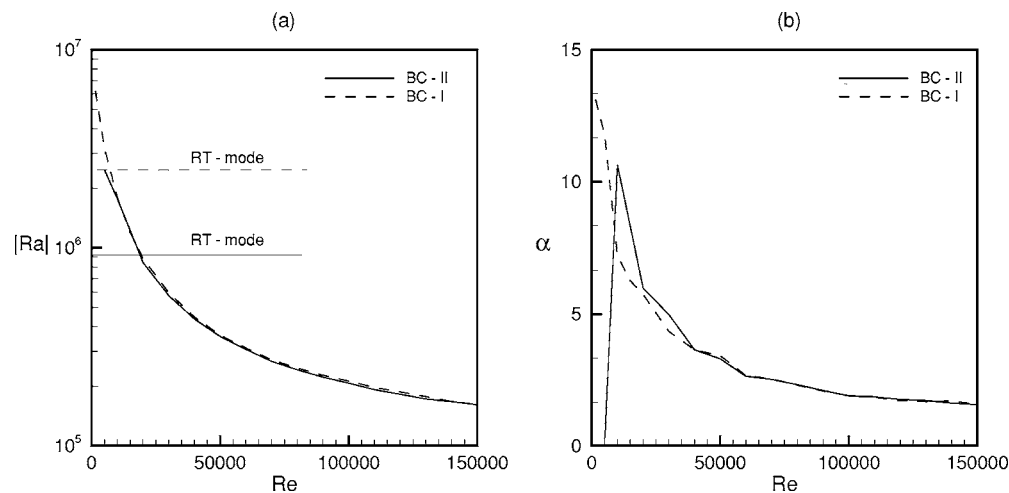
FIG. 9. Critical Rayleigh number (a) and wave number (b) as a function of Re under zero heat flux boundary condition for Pr=7 and Da=10^{-6}. Dashed lines show zero temperature boundary condition.

perturbation remains nonzero. A variation of critical Ra as a function of Re for the perturbed BC type I and BC type II are displayed in Fig. 9 for Da=10^{-6}, Pr=7. The dashed and solid lines in the (Re, |Ra|) plane and (Re, α) plane represent instability boundary curves for BC type I and BC type II, respectively. As can be seen from the figure, the base flow under BC-I remains slightly more stable compared to BC-II. For both BC-types, the difference between the critical Ra was significant for relatively small Re. Beyond this threshold value (Re=20 000), both BC-types led to the same results. Since, under BC-I, bounding walls are assumed to have high heat conductivity and heat capacity, it is expected that heat transfer by thermal diffusion will be comparable to the same under BC-II. Hence, thermal diffusivity suppresses the thermal fluctuations in the flow field. As a result, the flow remains stable even for larger values of Ra. Another important finding from this analysis is that the $R-T$ mode of instability for both BC-types differs significantly.

IV. CONCLUSIONS

We have attempted to understand of instability of buoyancy opposed, mixed convection in a vertical channel filled with a fluid-saturated porous medium. To this end, we adopted the Brinkman-Wooding-extended Darcy model. By means of linear theory, we were able to extract detailed information on the transition of basic flow through a porous medium for different fluids. The constant heat flux imposed on the walls was studied for two different temperature perturbations (namely zero temperature and zero heat flux). The main objective in this study was to investigate the effect of Prandtl number on the stability of base flow.

Furthermore, the basic flow stability was examined for the Pr range of [0.01,100]. As previously reviewed for buoyancy opposed flow of a viscous fluid (Scheele and Hanratty[27]), for pipe flows (Su and Chung[26]), for vertical annulus (El-Genk and Rao[28]), and for channel flow (Chen and Chung[22]), there are sudden and abrupt jumps. This was also true for a saturated porous medium. Furthermore, it was found that fully developed flow is most unstable for heavy oils (liquids with very large Pr). Scheele and Hanratty's[27] speculation that the instability in buoyancy opposed flows can be attributed to the appearance of point of separation is true only for fluids with Pr of O(1). The present study discloses that Pr plays an active role in buoyancy-opposed flows, and it is an indication for the viability of kinetic and thermal disturbances. Also, depending on the magnitude of all parameters studied, Rayleigh-Taylor and buoyant instabilities may occur. It was also observed that the energy spectrum profile at $\beta=0$ was gradual for Da=10^{-6}, and abrupt for Da=10^{-5}. The Rayleigh-Taylor mode of instability was operative for relatively small Re, and a direct link existed between the critical Ra in the Rayleigh-Taylor mode and Da given by −Ra Da=2.47. It is worth mentioning that beyond a certain value of Re, different types of boundary conditions on temperature did not alter the buoyant stability, whereas they did modify the Rayleigh-Taylor instability significantly.

[1] N. G. Holm, A. G. Cairns-Smith, R. M. Daniel, J. P. Ferris, R. J. C. Hennet, E. L. Shock, B. R. T. Simoneit, and H. Yanagawa, "Future research," in *Marine Hydrothermal Systems and the Origin of Life*, edited by N. G. Holm (Kluwer Academic, Dordrecht, 1992).
[2] P. R. Dando, A. Hughes, Y. Leahy, S. J. Niven, L. J. Taylor, and C. Smith, "Gas venting rates from submarine hydrothermal areas around the island of Milos, Hellenic Volcanic Arc," Cont. Shelf Res. **15**, 913 (1995).
[3] P. R. Dando, D. Stúben, and S. P. Varnavas, "Hydrothermalism in the Mediterranean Sea," Prog. Oceanogr. **44**, 333 (1999).
[4] D. A. Nield and A. Bejan, *Convection in Porous Media* (Springer-Verlag, New York, 2006).
[5] M. Parang and M. Keyhani, "Boundary effects in laminar mixed convection flow through an annular porous medium," ASME J. Heat Transfer **109**, 1039 (1987).
[6] K. Muralidhar, "Mixed convection flow in a saturated porous annulus," Int. J. Heat Mass Transfer **32**, 881 (1989).
[7] A. Hadim and G. Chen, "Non-Darcy mixed convection in a vertical porous channel with asymmetric wall heating," J. Thermophys. Heat Transfer **8**, 805 (1994).

[8]Y. C. Chen, J. N. Chung, C. S. Wu, and Y. F. Lue, "Non-Darcy mixed convection in a vertical channel filled with a porous medium," Int. J. Heat Mass Transfer **43**, 2421 (2000).

[9]P. Bera and A. Khalili, "Stability of mixed convection in anisotropic porous channel," Phys. Fluids **14**, 1617 (2002).

[10]Y. C. Chen, "Non-Darcy flow stability of mixed convection in a vertical channel filled with a porous medium," Int. J. Heat Mass Transfer **47**, 1257 (2004).

[11]M. Kaviany, *Principles of Heat Transfer in Porous Media* (Springer-Verlag, New York, 1995).

[12]R. A. Wooding, "Steady state free thermal convection of liquid in a saturated permeable medium," J. Fluid Mech. **2**, 273 (1957).

[13]K. Vafai, "Convective flow and heat transfer in variable-porosity media," J. Fluid Mech. **147**, 233 (1984).

[14]V. Prasad, F. A. Kulacki, and M. Keyhani, "Natural convection in porous media," J. Fluid Mech. **150**, 89 (1985).

[15]N. Martys, D. P. Bentz, and E. J. Garboczi, "Computer simulation study of the effective viscosity in Brinkman's equation," Phys. Fluids **6**, 1434 (1994).

[16]A. J. Basu and A. Khalili, "Computation of flow through fluid-sediment interface in a benthic chamber," Phys. Fluids **11**, 1395 (1999).

[17]A. Khalili, A. J. Basu, U. Pietrzyk, and M. Raffel, "An experimental study of recirculating flow through fluid-sediment interfaces," J. Fluid Mech. **383**, 229 (1999).

[18]D. F. James and A. M. J. Davis, "Flow at the interface of a model fibrous porous medium," J. Fluid Mech. **426**, 47 (2001).

[19]R. C. Givler and S. A. Altobelli, "A determination of the effective viscosity for the Brinkman–Forchheimer flow model," J. Fluid Mech. **258**, 355 (1994).

[20]T. S. Lundgren, "Slow flow through stationary random beds and suspensions of spheres," J. Fluid Mech. **51**, 273 (1972).

[21]P. G. Drazin and W. H. Reid, *Hydrodynamic Stability* (Cambridge University Press, Cambridge, 1981).

[22]Y. Chen and J. N. Chung, "The linear stability of mixed convection in a vertical channel flow," J. Fluid Mech. **325**, 29 (1996).

[23]J. C. Ward, "Turbulent flow in porous media," J. Hydr. Div. **90**, 1 (1964).

[24]R. B. Pandey and J. L. Becklehimer, "Computer simulation study of the permeability of a porous sediment model," Phys. Rev. E **51**, 3341 (1995).

[25]L. S. Yao and B. B. Rogers, "The linear stability of mixed convection in a vertical annulus," J. Fluid Mech. **201**, 279 (1989).

[26]Y. C. Su and J. N. Chung, "Linear stability analysis of mixed-convection flow in a vertical pipe," J. Fluid Mech. **422**, 141 (2000).

[27]G. F. Scheele and T. J. Hanratty, "Effect of natural convection on stability of flow in a vertical pipe," J. Fluid Mech. **14**, 244 (1962).

[28]M. S. El-Genk and D. V. Rao, "Buoyancy induced instability of laminar flows in vertical annuli—I. Flow visualization and heat transfer experiments," Int. J. Heat Mass Transfer **33**, 2145 (1990).